JACS Au
AN OPEN ACCESS JOURNAL OF THE AMERICAN CHEMICAL SOCIETY

pubs.acs.org/jacsau
Article

Direct or Precursor-Mediated? Mechanisms for Methane Dissociation on Pt(110)-(2 × 1) at Both Low and High Incidence Energies

Fenfei Wei, Sen Lin,* and Hua Guo*

Cite This: *JACS Au* 2023, 3, 2835−2843
Read Online
ACCESS | Metrics & More | Article Recommendations

ABSTRACT: The activation of alkanes on metal catalysts may involve a precursor-mediated mechanism, in which impinging molecules are first trapped on the catalyst surface to form an adsorbed precursor and may undergo extensive excursion on the surface in search of an active site. A characteristic feature of such a mechanism is an increasing initial sticking probability (S_0) with decreasing incidence energy at low incidence energies. Indeed, such "negative activation" was observed on the reconstructed Pt(110)-(2 × 1) surface with a missing row structure. In this paper, we describe an extensive theoretical investigation of methane dissociation on Pt(110)-(2 × 1) using a machine-learned high-dimensional potential energy surface (PES) based on a first-principles training data set. Quasi-classical trajectories (QCTs) are calculated on the PES to simulate the dissociation of both CH_4 and CHD_3 at various incidence energies. The agreement with the measured initial sticking probabilities is shown to be substantially improved for high incidence energies when compared to previous theoretical studies, indicating a better characterization of the dissociation barrier. Additional QCT calculations have been carried out for the trapping and diffusion of CHD_3 under experimental conditions at low incidence energies. The trapping probability is shown to increase with decreasing incidence energy, consistent with the experimentally observed "negative activation" below 10 kJ/mol. The reactivity of the trapped methane is attributed to the combined effect of its nonthermal diffusion across the surface Pt rows and the lowered barrier reached by surface thermal fluctuation. These simulations shed valuable light on the microscopic dynamics of the initial and often rate-limiting step in heterogeneous catalytic processes involving alkanes.

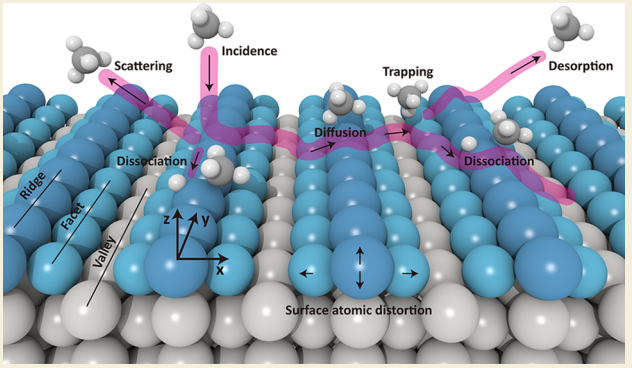

KEYWORDS: *dissociative chemisorption, precursor-mediated mechanism, surface dynamics, surface reaction, potential energy surfaces, molecular dynamics*

1. INTRODUCTION

A major problem that affects both social progress and quality of life is the sustainable use and conversion of energy. The activation of alkanes is an important field of current study for their effective usage as fuels and more importantly for their transformation into value-added products.[1,2] In many heterogeneous catalytic processes, such as steam and dry reforming of methane (CH_4), dissociative chemisorption is believed to be the initial and rate-limiting step.[3] To understand the microscopic mechanism, it is important to investigate the process under highly controlled conditions.[4] To this end, much work has recently been done for methane dissociation on low-Miller index metal surfaces in high vacuum with molecular beams.[5,6] These studies have often focused on using high incidence energies and/or vibrational excitation to overcome the relatively high activation barrier (∼100 kJ/mol). Under such circumstances, the dissociation was found to be direct and mode-specific, which is also confirmed by theoretical studies.[7,8]

In industrial processes, however, the incidence energy is often much lower than those used in laboratory studies. Under the reforming condition (700−1000 °C), the peak of the Maxwell−Boltzmann distribution of methane is about 10 kJ/mol. Hence, the activation process may follow more complex pathways than the direct mechanism mentioned above, which could be significantly influenced by energy transfer. Indeed, it

Received: July 18, 2023
Revised: August 24, 2023
Accepted: August 25, 2023
Published: September 18, 2023

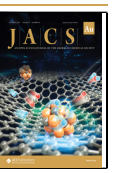

https://doi.org/10.1021/jacsau.3c00387
JACS Au 2023, 3, 2835−2843

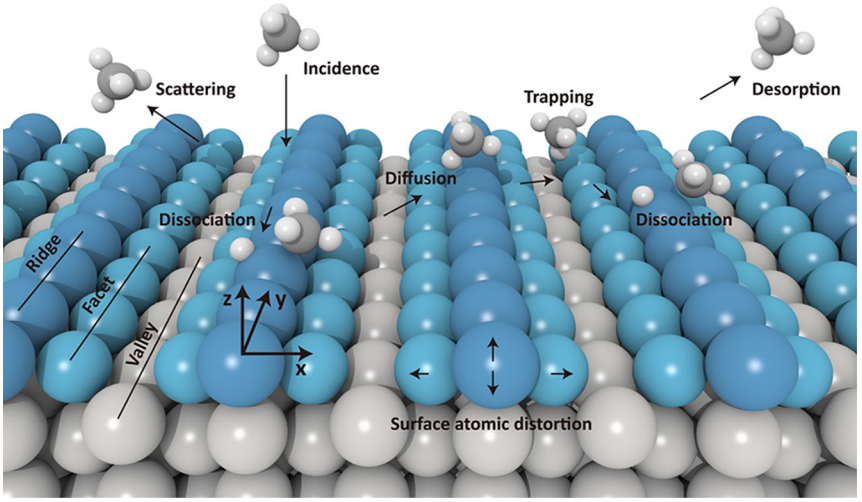

Figure 1. Schematic illustration of scattering, trapping, diffusion, dissociation, and desorption of methane on the Pt(110)-(2 × 1) surface. The coordinate system and the type of surface atoms (ridge, facet, and valley) are also defined.

has been demonstrated that the methane initial sticking probability (S_0) increases with decreasing incidence energy on hot Ir surfaces below 15 kJ/mol,[9−12] which is relevant to the industrial conditions. This so-called "negative activation" is in sharp contrast to the behavior at higher incidence energies, where the sticking probability increases with increasing incidence energy, and is attributable to the so-called precursor-mediated (PM) mechanism.[9,10] At these low incidence energies, the methane molecule impinging on the surface is first trapped in a physisorbed state and the reaction precursor subsequently undergoes nonthermal diffusion on the surface. When it encounters an active site with a relatively low barrier, dissociation occurs. Since the trapping probability increases with decreasing incidence energy, the reactivity follows.

This picture is supported by recent theoretical simulations,[13−17] in which facile trapping at low incidence energies and extensive roaming of the adsorbed CH_4 were seen on Ir surfaces. This is made possible by a relatively deep adsorption well (∼25 kJ/mol) on Ir surfaces. Despite energy loss to surface atoms along the surface normal, which is responsible for trapping, dissipation of kinetic energy along the surface plane is relatively slow, thanks to small diffusion barriers, leading to rapid and far-ranged diffusion of the adsorbate precursor. The extensive roaming of the precursor on the surface eventually leads to an encounter with an active site where the barrier is sufficiently low to permit dissociation. The low activation energy can, for example, be provided by the puckering of a surface atom, which lowers the dissociation barrier.[18] Indeed, Busnengo and co-workers proposed based on their simulations that thermal fluctuations of surface atoms on Ir(111) are responsible for transient active sites for methane dissociation,[14,16] which is consistent with the experimentally observed temperature effect. Our own simulations and those by Jackson however emphasized a more prominent role of defects in activating the trapped methane.[15,17,19]

Interestingly, "negative activation" has also been observed by Walker and King on Pt(110)-(2 × 1) for methane incidence energies below 20 kJ/mol.[20,21] The reconstructed Pt(110) surface has a missing row structure (Figure 1) and is a prototype for catalysis by highly corrugated surfaces, serving as a model for defects due to the undercoordinated Pt atoms at the ridge of each row. Later studies by Beck and co-workers also reported a similar observation below 10 kJ/mol.[22] This behavior is in stark contrast to that at higher incidence energies, in which the sticking probability increases with both the incidence energy and vibrational excitation.[22−24] The increasing sticking coefficient with decreasing incidence energy was initially attributed by Walker and King to a "dynamical steering assisted" (DSA) mechanism, which differs from the PM mechanism. In the DSA mechanism, the impinging methane molecule is thought to "steer" to a special orientation leading to a low (or null) barrier reaction path. Since the effectiveness of this steering force is inversely proportional to the incidence energy, the enhancement would only occur at low incidence energies.

However, density functional theory (DFT) calculations showed that the dissociative chemisorption of methane on Pt(110)-(2 × 1) has significant barriers (∼65 to 70 kJ/mol) at various surface sites,[24−29] thus discounting the possibility of direct reactions at low incidence energies, with or without steering. Dynamical calculations at large incidence energies[24,27−29] reproduced the experimental trends observed by Beck and co-workers,[22−24] confirming a direct mechanism. However, existing simulations using ab initio molecular dynamics (AIMD)[24] and a DFT-based reactive force field (RFF)[28] underestimated the experimental S_0, suggesting an overestimation of the dissociation barrier. To correct this problem, we have recently tested several functionals for methane dissociative chemisorption on the Pt(110)-(2 × 1) surface and identified some that are capable of reproducing the experimentally measured sticking probabilities thanks to their lower barriers.[29]

So far, all theoretical simulations have been restricted to relatively high incidence energies, where the direct mechanism dominates. No systematic investigations have been carried out to provide an explanation of the "negatively activated" dissociation of methane observed at low incidence energies.[20−22] This is because such simulations are quite difficult due to the long time nature of the trapping and diffusion processes. To answer this challenge, we in this work report the development of a high-dimensional potential energy surface (PES) for this system, machine-learned from DFT training data using one of the identified functionals. We demonstrate

https://doi.org/10.1021/jacsau.3c00387
JACS Au 2023, 3, 2835−2843

that this PES, with a high-fidelity representation of the new DFT data, semiquantitatively reproduces the existing experimental results at high incidence energies, thus providing a reliable platform for understanding the dissociation dynamics at both high and low incidence energies. We further investigate the scattering and trapping dynamics of methane at low incidence energies and present evidence that reactive events could indeed occur for trapped precursors. This conclusion provides a plausible explanation of all experimental observations, shedding light on the complex dynamics of this key surface reaction.

2. METHODS

2.1. Density Functional Theory

As mentioned above, most previous theoretical studies have underestimated the sticking probability for methane dissociation on Pt(110)-(2 × 1) at high incidence energies,[24,28] suggesting that the calculated barriers are probably too high. Tests we recently conducted have shown that the barriers depend sensitively on the functional used in DFT calculations.[29] AIMD simulations using a generalized gradient approximation (GGA) functional with nonlocal van der Waals correction, namely, optPBE-vdW,[30] and a made-simple meta-GGA functional,[31] namely, MS-PBEl-rVV10,[32] were performed at the experimental incidence energies,[24] which led to a much better agreement with the measured sticking probabilities.[29] Both functionals yielded lower barriers than those found in previous theoretical studies. Since the meta-GGA functional is associated with much higher computational costs, we have chosen to use the optPBE-vdW functional to describe the current system.

In the periodic DFT calculations, the Kohn−Sham orbitals were expanded into plane waves up to a cutoff energy of 400 eV and the ionic core was approximated by the projector augmented wave (PAW) method.[33] A 1 × 3 unit cell of Pt(110)-(2 × 1) was used under periodic boundary conditions in all calculations. The top four atomic layers in the seven atomic layer slab were relaxed and a vacuum distance of 20 Å was employed along the Z-direction to avoid interactions between the periodic images. The Brillouin zone was sampled using a 3 × 3 × 1 Monkhorst−Pack k-point grid.[34] Transition states were determined by the climbing-image nudged elastic band (CI-NEB) method.[35] All spin nonpolarized DFT calculations were performed with the Vienna Ab initio Simulation Package (VASP).[36,37]

The adsorption energy of methane (E_{ads}) and its dissociation barrier (E_b) are defined as follows:

$$E_{ads} = E_{(molecule+surface)} - E_{(surface)} - E_{(molecule)} \quad (1)$$

$$E_b = E_{(transition\ state)} - E_{(surface)} - E_{(molecule)} \quad (2)$$

where $E_{(molecule\ +\ surface)}$, $E_{(surface)}$, and $E_{(molecule)}$ represent the energies of methane adsorption configuration, the bare surface, and the free methane molecule. The transition state energy $E_{(transition\ state)}$ for methane dissociation was measured from the gas-surface asymptote.

Additional AIMD calculations were performed in which the initial conditions, including the surface temperature (T_s) and the incidence energy and angle, were selected to mimic the experimental conditions.[24,28] Specifically, the temperature T_s of the Pt(110)-(2 × 1) surface was set at 650 K and the surface coordinates and momenta obtained after equilibration under the NVE ensemble for 4 ps with a 1 fs time step were used.

2.2. Construction of Potential Energy Surfaces

The row-deficient reconstructed Pt(110)-(2 × 1) surface is highly corrugated and anisotropic, as depicted in Figure 1. It provides several types of surface atoms, many of which are unsaturated. This leads to multiple adsorption and reaction sites,[26] which pose a challenge for a high-fidelity representation of the potential landscape. Our DFT model contains 26 mobile atoms in the super cell, including 21 surface atoms and five atoms from CH_4. The 78-dimensional PES was represented by the embedded atom neural network (EANN) approach,[38] which has been successfully applied in many gas/solid interfacial reactions.[39,40] The data set was mainly from the AIMD simulations reported in our earlier work.[29] Additional static DFT and AIMD calculations were performed to supplement the original data set, as detailed below.

In the EANN approach,[38] the total energy of the system is expressed as the sum of atomic energies:

$$E = \sum_{i=1}^{N} E_i = \sum_{i=1}^{N} NN_i(\rho^i) \quad (3)$$

each of which is an output of an atomistic NN. ρ^i represents the density-like feature vector of the central atom i and its component is evaluated by the square of a linear combination of Gaussian-type orbitals (GTOs) located at neighbor atoms. $\varphi^{\alpha,r_s}_{l_x l_y l_z}(\mathbf{r}_{ij})$ represents GTOs:

$$\rho^i = \sum_{l_x,l_y,l_z}^{l_x+l_y+l_z=L} \frac{L!}{l_x!l_y!l_z!}\left(\sum_{j\neq 1}^{N_c} c_j \varphi^{\alpha,r_s}_{l_x l_y l_z}(\mathbf{r}_{ij}) f_c(\mathbf{r}_{ij})\right)^2 \quad (4)$$

$$\varphi^{\alpha,r_s}_{l_x l_y l_z}(\mathbf{r}_{ij}) = x^{l_x} y^{l_y} z^{l_z} \exp(-\alpha |r_{ij} - r_s|^2) \quad (5)$$

Here, N_c is the number of neighboring atoms within a cutoff radius (r_c) to the central atom, $f_c(\mathbf{r}_{ij})$ is a cutoff function to ensure that the contribution of each neighboring atom decays smoothly to zero at r_c, and c_j serves like an orbital coefficient of atom j that is element-dependent and optimized along with the training process. r_{ij} is the distance between atoms i and j, and α and r_s are parameters that determine radial distribution of the GTO. $l_x + l_y + l_z = L$ specifies the orbital angular momentum (L) and the angular distribution of the GTO.

The NN structure of 60 × 30 × 60 × 1 was used for each atom with two hidden layers. The penalty function is given in ref 38, which includes both the potential energy and gradient. To avoid overfitting, the data set was separated into a training set and a verification set. The optimization of the fitting is considered convergent when the decreases of the cost function of continuous six steps are all less than the criteria of 0.0965 kJ/mol and the error in the verification set is larger than that in the training set. The nonlinear optimization was carried out using the Levenberg−Marquardt algorithm.[41]

2.3. Quasi-Classical Trajectory Calculations

The quasi-classical trajectory (QCT) method was used to characterize the dynamics as implemented in a user-modified[42] version of the VENUS code.[43] The distance of the molecular center of mass (COM) of CHD_3 or CH_4 to the surface was initialized at 6 Å, where the surface was taken to be at the average height (Z-coordinate) of the ridge Pt atoms. The vibrational distribution was sampled either with the Boltzmann distribution at the nozzle temperature (T_N), even though the distribution might not be Boltzmann, or at a vibrational excited state. The zero-point energy was set as zero for vibration. The rotational quantum number was set to zero because the effect of rotation is small based on a previous report.[20] A series of incidence energies (E_i) along the surface normal were used and 50,000 trajectories were propagated for each high incidence energy. Each trajectory was propagated until either the molecule is scattered, dissociated, or reached the 10 ps propagation time. A trajectory was considered reactive if a C−H bond distance (or one of the C−D bond distances in CHD_3) exceeded 2.2 Å or scattered when the COM of CHD_3 or CH_4 was more than 6.0 Å above the surface. If a trajectory leads to neither dissociation nor scattering after the 10 ps propagation time, the molecule was considered trapped. For low E_i (1.3, 4.0, and 12.6 kJ/mol), the trapped trajectories were propagated further for a total of 66 ps. To obtain meaningful statistics, 300,000 trajectories were computed at each low incidence energy.

https://doi.org/10.1021/jacsau.3c00387
JACS Au 2023, 3, 2835−2843

Table 1. Comparison of the Adsorption Energy (E_{ads}) and Dissociation Barrier (E_b) (kJ/mol) for Methane at the Ridge, Facet, and Valley Sites on the Pt(110)-(2 × 1) Surface Obtained by DFT with the optPBE-vdW Functional and PES[a]

site	E_{ads} (DFT)	E_{ads} (PES)	E_b (DFT)	E_b (PES)	E_b[b]	E_b[c]	E_b[d]	E_b[e]
ridge (K1)	−19.1	−18.6	53.4	54.1	68.5	67.5	69.8	59.8
ridge (K2)	−19.0	−18.6	56.2	55.7	71.4	69.5		61.8
ridge (L1)	−19.7	−19.0	46.7	47.4	71.4	69.5		59.8
ridge (L2)	−20.3	−20.7	45.6	45.3	70.4	68.5	63.9	58.9
facet (TS3)			63.7	63.3			94.8	
valley (TS3)	−28.4	−28.9						

[a]The nomenclature of four adsorption modes on the ridge denotes the orientation of methane, following the previous work.[26] For the transition state (TS3) at a facet site,[24] the corresponding adsorption site is at a valley site. [b]Rigid surface, PBE functional, ref 28. [c]Rigid surface, PBE functional, ref 27. [d]Rigid surface, SRP32-vdW functional, ref 24. [e]Nonrigid surface, PBE functional, ref 28.

3. RESULTS AND DISCUSSION

3.1. PES Fitting

As mentioned above, the DFT data were from our previous AIMD calculations carried out at the experimental incidence energies of 124.6 and 106.8 kJ/mol for ro-vibrationally ground state of CHD_3 impinging on Pt(110)-(2 × 1) along the surface normal. In this work, we have calculated an additional 100 AIMD trajectories with CH_4 (v_3 = 1) at 650 K. This batch of AIMD trajectories provides data for the interaction of vibrationally excited methane with the surface. To further improve the description of the postdissociation dynamics, six dissociation trajectories at 106.8 kJ/mol of incidence energy were further propagated for 2 ps.

About 160,000 points were generated from the 200 AIMD trajectories reported in our earlier work,[29] and we have selected 5000 points using the K-Means method in the Python scikit-learn toolkit,[44] which updates the COM of the initial randomly generated data cluster by the distance between the data and the COM until the COM of the data cluster is unchanged. A primitive PES was then constructed using these points. To improve the PES, we have added additional points to the training set. First, trajectories were launched on this PES to explore regions not accessed by the initial AIMD trajectories. These regions were identified by the failure of energy convergence in QCT, and 2068 points were added in these regions. Second, 2633 points around different adsorption configurations and 1468 points along the dissociation pathway were added to the training data. Furthermore, 2500 points generated from another 100 AIMD trajectories for the impinging $CH_4(v_3 = 1)$ at E_i = 124.6 kJ/mol were selected using the same K-Means method and added. Finally, a total of 16,161 points were used as the training data set. These data points include both energies and gradients.

The root-mean-square error (RMSE) of the EANN PES is 1.3 kJ/mol for energy per cell (0.05 kJ/mol per movable atom) and 4.1 kJ/mol $Å^{-1}$ for force. The fitting error is about one order of magnitude lower than the reactive force field (RFF) approach,[28] due apparently to the flexibility of the NN. More importantly, the number of configurations is about 1.6 times of the RFF fitting,[28] which is expected to provide a better description of the PES. To demonstrate the high fidelity of the PES, energies for CH_4 adsorption and dissociation barriers obtained by DFT and PES are compared in Table 1.

It is clear from the table that methane adsorbs most strongly at valley sites, but the dissociation barrier is the lowest at ridge sites. We emphasize that the dissociation barriers in the PES are significantly lower than the previous theoretical values, for example, those reported in ref 28. These characteristics become important for understanding the dynamics of dissociation and diffusion.

3.2. Dissociation

In Figure 2, we compare the calculated dissociative sticking probability (S_0) of CHD_3 on Pt(110)-(2 × 1) at the experimental nozzle temperatures of Beck and co-workers[24] with a T_s of 650 K. It is clear that our calculated S_0 values based on 50,000 trajectories are in good agreement with the experimental results, particularly toward the high end of the incidence energy above 100 kJ/mol. At incidence energies near 60−70 kJ/mol, the calculated dissociation probabilities are somewhat lower than the experimental values but still within the error bounds. Our earlier AIMD values at two incidence energies using the same functional[29] are also in good agreement with the QCT results at the same energies but with larger uncertainties due to the much smaller number of

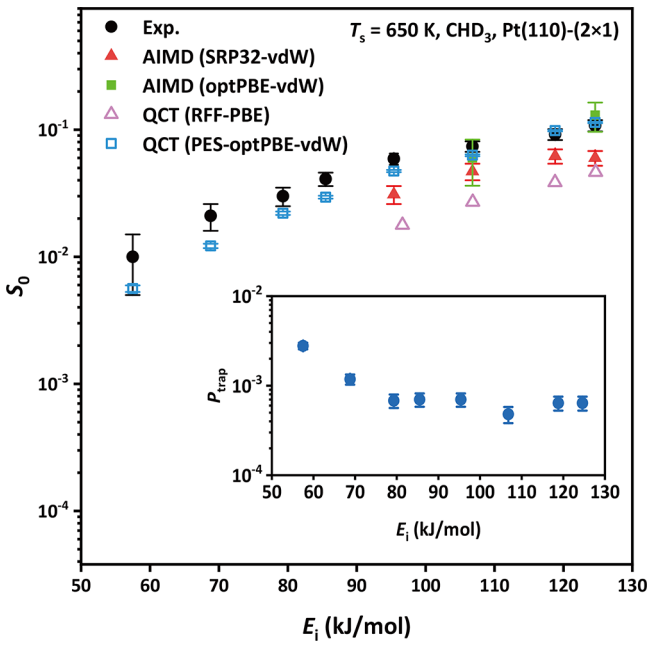

Figure 2. Comparison of QCT sticking probabilities (S_0) for CHD_3 dissociation on Pt(110)-(2 × 1) at several experimental incidence energies and a T_s of 650 K.[24] The previous AIMD results using the SRP functional[24] and QCT results on a PBE-based RFF[28] are included for comparison. In addition, the AIMD results from our earlier work using the same optPBE-vdW functional[29] are also included. The inset shows the trapping possibility of CHD_3 after 10 ps at a T_s of 650 K and experimental T_N as a function of the incidence energy E_i.

https://doi.org/10.1021/jacsau.3c00387
JACS Au 2023, 3, 2835−2843

trajectories. This agreement underscores the high fidelity of the EANN PES.

These new results in Figure 2 represent a significant improvement over the previous theoretical calculations, which are also included in the figure for comparison. While in qualitative agreement with the experimental data, both the AIMD results based on a special reaction parameter (SRP) functional,[24] which is a weighted sum of the PBE and RPBE functionals,[45] and the RFF results based on the PBE functional[28] significantly underestimated the experimental values. As discussed in our earlier work,[29] these quantitative discrepancies can be attributed to the overestimated reaction barriers for methane dissociation on the Pt(110)-(2 × 1) surface. Specifically, the barrier at the K1 site is 53.4 kJ/mol on the optPBE-vdW based PES, much lower than 64.6 kJ/mol[29] using the SRP functional or 59.8 kJ/mol from the PBE.

In addition to the dissociation and scattering trajectories, we have also observed some trapping. At the end of the 10 ps simulations, for example, there are still ∼0.1% of CHD_3 on the surface, as shown in the inset of Figure 2. This is consistent with the earlier simulation results of Peludhero et al.,[28] who found that ∼0.1% of the trajectories were trapped at 5 ps. However, few of the trapped trajectories led to a reaction and they make a negligible contribution to the total sticking probability, an observation that is also consistent with previous simulations.[28]

To understand the site specificity for methane dissociation on the Pt(110)-(2 × 1) surface, we divided the *X*-axis (perpendicular to the rows) with a 0.1 Å interval and calculated 500 trajectories in each interval. As shown in Figure 3, it is clear that most of the dissociation occurs at the ridge and facet sites, with almost no dissociation in the valley. At low incidence energies, the dissociation almost exclusively occurs at the ridge site. As the energy increases, the facet site becomes reactive as well. The dominance of the ridge site in methane dissociation is consistent with observations in previous experiments[22,46] and theoretical calculations.[24,28] It can be attributed to the fact that the ridge sites have lower barriers than the facet sites, with the valley sites not amenable to dissociation, as shown in Table 1.

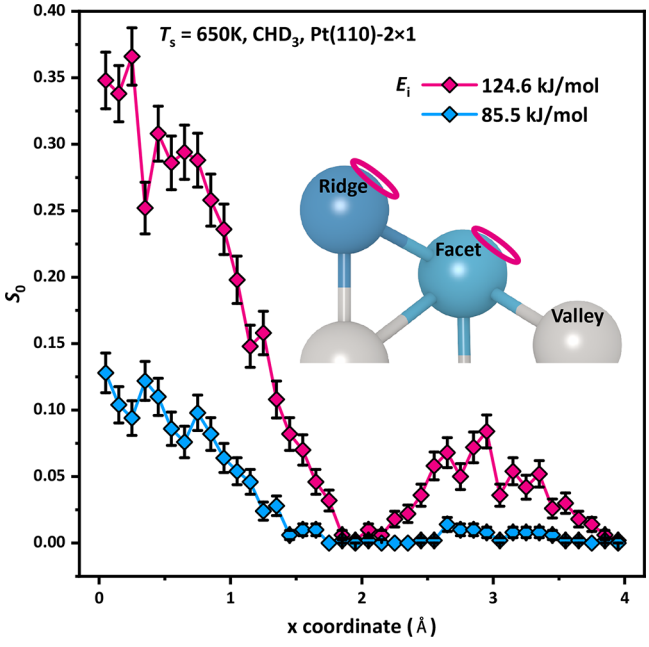

Figure 3. S_0 for CHD_3 dissociation at two incidence energies for different *Z* positions of the Pt(110)-(2 × 1) surface at a T_s of 650 K.The inset depicts the surface geometry along the *X*-coordinate with the red circles indicating the major active sites for dissociation.

Furthermore, we investigate the performance of the new PES in calculating the sticking probability of CH_4 under the experimental conditions at a T_s of 650 K, and the results are displayed in Figure 4. As in the CHD_3 case discussed above,

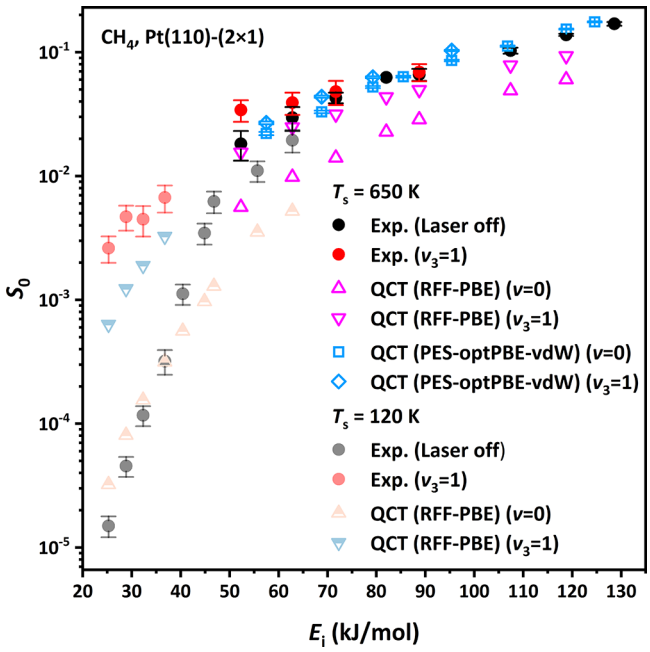

Figure 4. Comparison of QCT sticking probabilities (S_0) for CH_4 dissociation on Pt(110)-(2 × 1) at different incidence energies under the condition v = 0 and v_3 = 1 at a T_s of 650 K. The experimental results (laser-off and v_3 = 1)[28] and previous QCT results on a PBE-based RFF[28] at T_s of 120 and 650 K are included for comparison.

the agreement of the v = 0 theoretical results with the experimental data under the laser-off conditions[28] is quite good, much better than the previous theoretical calculations.[28] In addition, the sticking probability of CH_4 (v_3 = 1) is found to be higher than the ground vibrational counterpart, consistent with experimental observations. The better agreement with the experiment in both cases is mainly attributable to the different functionals (optPBE-vdW vs PBE) used in the two theoretical approaches. Also, we observed that the dissociation probability is lower at a low T_s than that at a high T_s under the same E_i. Additionally, the S_0 when v_3 = 1 using QCT is slightly lower than that of the experiment at T_s = 650 K. These results provide further supporting evidence for the accuracy of the PES in describing the dissociative chemisorption of methane on Pt(110)-(2 × 1).

3.3. Trapping and Diffusion

We performed QCT calculations on the same PES at the CHD_3 incidence energies of 1.3, 4.0, and 12.6 kJ/mol, with other initial conditions remaining the same. At these energies, the majority of the 300,000 trajectories are trapped and undergo extensive diffusion on the surface. This is made possible by the deep adsorption well (−28.4 kJ/mol) on the Pt surface (Table 1). To follow the long trapping dynamics, the trapped trajectories were propagated for 66 ps, which is the

https://doi.org/10.1021/jacsau.3c00387
JACS Au 2023, 3, 2835−2843

lifetime estimated in previous theoretical work.[24] Such long-time propagation would have been extremely difficult with AIMD but manageable with the NN PES. As shown in Figure 5, the initial trapping probability decreases with the incidence

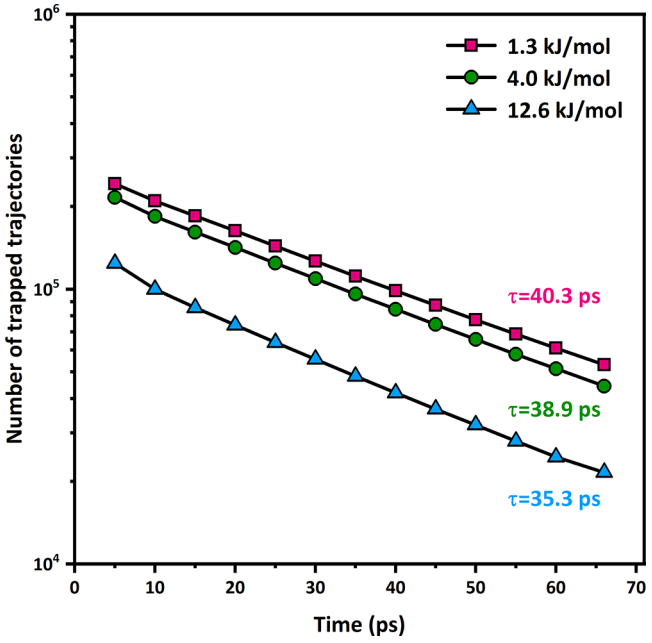

Figure 5. Number of trapped CHD_3 on Pt(110)-(2 × 1) as a function of time at a T_N of 600 K at several lower incidence energies. The lifetimes are given assuming the first-order kinetics.

energy. This is expected as the impinging molecule with a lower incidence energy has a better chance of being trapped on the surface. Furthermore, the number of trapped trajectories is largely an exponentially decaying function of time, which suggests first-order desorption kinetics. The lifetimes at three incidence energies are labeled in the figure, which show that the trapping at this surface temperature (650 K) persists a few tens of picoseconds. In addition, the data in the figure indicate that the lifetime decreases with the incidence energy.

It is interesting to note that trapping is a dynamical process. Instead of staying in the impact site, the physisorbed molecule undergoes extensive migration on the surface, driven by the COM momentum along the surface plane gained upon impact with the surface. Such nonthermal diffusion has been observed during methane collisions on Ir surfaces,[13−17] which also have a relatively deep adsorption well.

Furthermore, the diffusion of the translationally "hot" methane on Pt(110)-(2 × 1) is highly anisotropic, with a much longer diffusion length along the *Y*-axis than along the *X*-axis. In Figure 6a, the averaged displacement distances along the two directions are plotted as a function of time. Within the 66 ps, the averaged displacement along the *Y*-axis is approximately 120 Å, while that along the *X*-axis is only 30 Å. Similar diffusion anisotropy was observed in the recent simulations by Busnengo and co-workers using their RFF.[28] This strong anisotropy is dictated by the PES, which is shown in Figure 6b where adsorption energy of CH_4 with one-H down configuration is shown as a function of the *X*- and *Y*-coordinates. The adsorption energy along the valley is −27.0 kJ/mol, which is much larger than that at the top site of the ridge Pt atom (−19.5 kJ/mol). More importantly, the diffusion barrier along the *Y*-axis is essentially zero (~0.2 kJ/mol). This

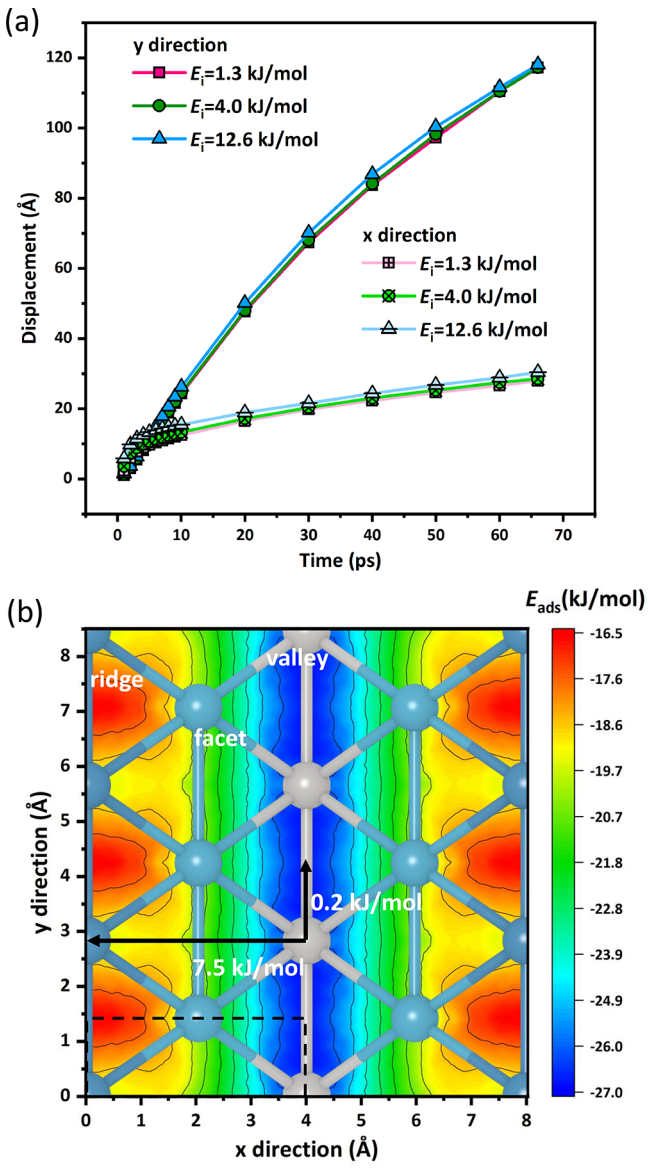

Figure 6. (a) Average displacement of CHD_3 as a function of time for diffusion in the *X*- and *Y*-directions at an E_i of 1.3, 4.0, and 12.6 kJ/mol. The distance is measured from the initial impact site to the COM of CHD_3. (b) Potential energy surface in the *X*−*Y* plane for the COM of methane with one-H down on relaxed Pt(110)-(2 × 1), with the height and rotation angle of methane relaxed. The diffusion barriers in both directions are shown.

explains the extensive diffusion along the *Y*-axis shown in Figure 6a. On the other hand, the diffusion along the *X*-axis is subjected to a much larger energy cost (7.5 kJ/mol) from the valley site to the top site, leading to a much shorter diffusion length. It is important to note that the diffusion along the valley does not contribute to the reactivity because the dissociation barriers are at the ridge and facet sites. On average, the molecule crosses about three ridges during the 66 ps propagation.

3.4. Precursor-Mediated Dissociation

The QCT results at low incidence energies are clearly dominated by trapping, which has a negative dependence on the incidence energy. Among the 300,000 trajectories at the three low incidence energies, however, there were only a few reactive ones, corresponding to a sticking probability of ~10^{-5}.

https://doi.org/10.1021/jacsau.3c00387
JACS Au 2023, 3, 2835−2843

Table 2. Initial Sticking Probability and the Numbers of Direct and Indirect Reactive Trajectories at Incidence Energies of 1.3, 4.0, and 12.6 kJ/mol for CHD_3 (T_N of 600 K) Impinging on the Pt(110)-(2 × 1) Surface at a T_s of 650 K[a]

E_i (kJ/mol)	S_0	total number of reactive trajectories	direct (%)	indirect(%)	average Q_Z (Å)
1.3	$(3.0 \pm 1.0) \times 10^{-5}$	10	20.0	80.0	0.366
4.0	$(1.6 \pm 0.7) \times 10^{-5}$	5	60.0	40.0	0.267
12.6	$(6.0 \pm 1.0) \times 10^{-5}$	18	83.3	16.7	0.306

[a]The average vertical displacements of the active ridge Pt atom (Q_Z) for reactive trajectories are given in Å.

While the statistics are still insufficient, the estimated S_0 from these calculations is not inconsistent with the experimental evidence, in which the sticking probability is on the order of 10^{-6}–10^{-7} for an incidence energy of 10 kJ/mol.[22] More importantly, some of the dissociation observed in our simulation was indirect, namely, the dissociation occurred after a significant time in the adsorbed state. The explicit observation of these dissociation events in our simulations is strong supporting evidence of the PM mechanism. Interestingly, the indirect portion increases with the decreasing incidence energy, consistent with expectation. The results are summarized in Table 2.

Given the low reactivity, a converged simulation of the dissociation dynamics via the PM mechanism is beyond our current abilities, as it requires a much larger number ($\gg 10^6$) of long trajectories. However, it is possible to speculate the chances of such events from the existing knowledge of the system. It is well established that the puckering of a surface atom lowers the dissociation barrier for methane.[26,27] Such puckering can be facilitated by the thermal fluctuation of the surface. To quantify this effect, the dissociation barrier at the L2 site is calculated as a function of the position of the underlying ridge Pt atom along the Z-direction (Q_z) and is shown in Figure 7a. It is clear that the movement of the Pt atom above the surface plane lowers the barrier from 45.6 kJ/mol at equilibrium to 23.3 kJ/mol at Q_Z = 0.4 Å. This dependence on the surface atom displacement is consistent with the earlier calculations of the same process by Jackson and co-workers.[27]

In Figure 7b, the thermal fluctuations of the surface atoms along the Z-direction are displayed. These results were obtained with an NVT simulation at a surface temperature of 650 K. It is clear from the figure that the ridge atoms have on average larger displacements than the facet atoms. This fluctuation results in a small but finite population of ridge atoms near Q_Z = 0.4 Å, which could provide the necessary active site. In fact, the average vertical displacements of the active ridge Pt atom in the few dissociation trajectories in our low-energy simulations suggest that this scenario is indeed viable (see Table 2), albeit with small probabilities with large uncertainties due to limited number of trajectories. This is also consistent with the experimentally observed significant temperature dependence of the sticking probability[22] and its theoretical interpretation.[27] Unfortunately, a quantitative simulation of such PM events would require orders of magnitude larger computational costs.

We further argue that the experimentally observed dissociation at low incidence energies might also be assisted by other defects on the reconstructed Pt surface. There is ample evidence suggesting that surface defects with low reaction barriers might contribute to a significant portion of the reactivity, even when they constitute only a fraction of the surface sites.[47,48] In the case of methane dissociation on Ir surfaces, theoretical results strongly suggest that step defects

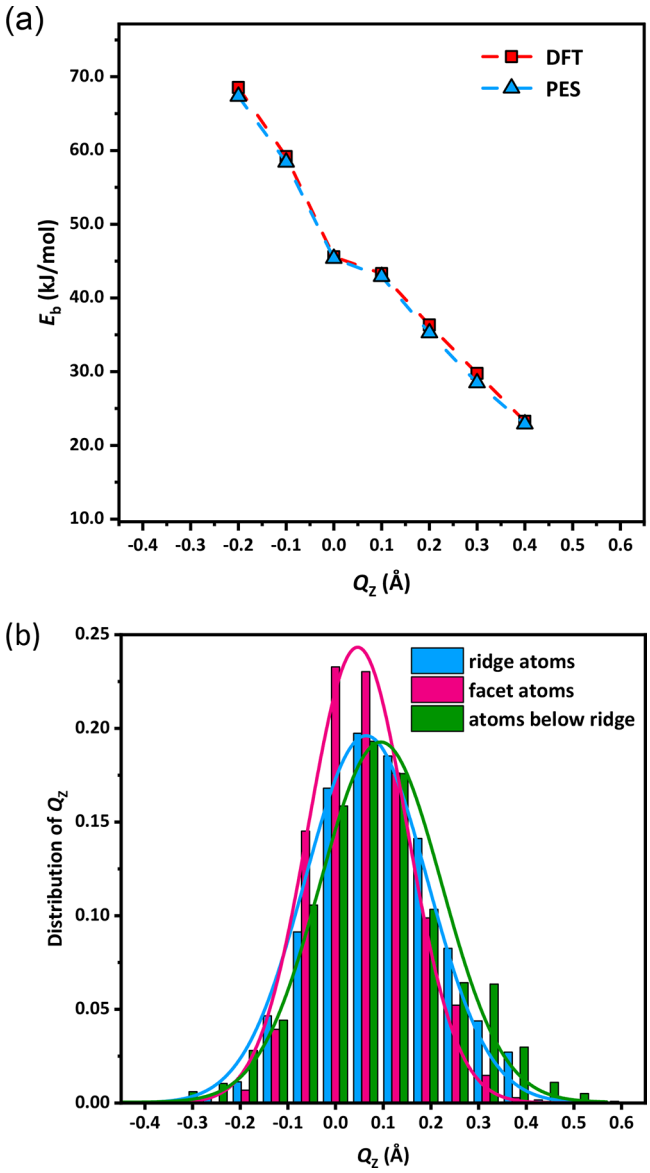

Figure 7. (a) Dependence of the dissociation barrier (E_b) with the vertical distortion of the surface ridge Pt atom below methane (Q_Z), calculated directly from DFT and using the PES. (b) Thermal fluctuations of surface atoms of Pt(110)-(2 × 1) at 650 K.

strongly promote the PM mechanism.[15,17,19] Furthermore, other high-index steps and kinks may also exhibit lower methane activation energies and can serve as potential active sites. However, this requires further in-depth exploration.

4. CONCLUSIONS

In the current study, we report the construction of a high-dimensional PES for methane dissociation on the Pt(110)-(2 × 1) surface. This PES is machine-learned from a large number

https://doi.org/10.1021/jacsau.3c00387
JACS Au 2023, 3, 2835−2843

of DFT data obtained using the optPBE-vdW functional. Quasi-classical trajectory calculations on this new PES yield sticking probabilities for both CH_4 and CHD_3 at high incidence energies in better agreement with the latest experiment than previous theoretical reports. Analysis of the trajectories shows that the dissociation at these incidence energies is direct and mode-specific. The reaction mostly occurs at ridge sites, with some at facet sites.

At low incidence energies, there is significant trapping, thanks to energy loss to the surface. The relatively deep adsorption well results in a long trapping lifetime (10−100 ps) even at relatively high surface temperatures. The trapping probability is inversely proportional to the incidence energy, consistent with the experimentally observed "negative activation" at low energies. The dissociation via the precursor-mediated mechanism is likely facilitated by transient active sites on the surface, resulted from thermal fluctuations of ridge atoms or defects. These active sites are explored by the roaming adsorbates, which are slow in reaching thermal equilibrium with the surface. Indeed, the trapped precursor is found to undergo extensive nonthermal diffusion and the diffusion is anisotropic, dictated by the lack of significant diffusion barriers along the valley between two rows of Pt atoms. The average diffusion distance along the valley is about six times longer than that across the rows. However, the latter is responsible for the precursor-mediated dissociation, as the dissociation transition states are the lowest at the ridge sites. Although our simulations are insufficient to provide a quantitative determination of the sticking probability at low incidence energies, they offer tantalizing evidence for a better understanding of the low-energy reactivity of this prototypical heterogeneous reaction.

AUTHOR INFORMATION

Corresponding Authors

Sen Lin − *State Key Laboratory of Photocatalysis on Energy and Environment, College of Chemistry, Fuzhou University, Fuzhou 350002, China;* orcid.org/0000-0002-2288-5415; Email: slin@fzu.edu.cn

Hua Guo − *Department of Chemistry and Chemical Biology, University of New Mexico, Albuquerque, New Mexico 87131, United States;* orcid.org/0000-0001-9901-053X; Email: hguo@unm.edu

Author

Fenfei Wei − *State Key Laboratory of Photocatalysis on Energy and Environment, College of Chemistry, Fuzhou University, Fuzhou 350002, China*

Complete contact information is available at: https://pubs.acs.org/10.1021/jacsau.3c00387

Notes

The authors declare no competing financial interest.

ACKNOWLEDGMENTS

F.W. and S.L. acknowledge financial support from the National Natural Science Foundation of China (Grant Nos. 22373017 and 21973013), the National Natural Science Foundation of Fujian Province, China (Grant No. 2020J02025), and the "Chuying Program" for the Top Young Talents of Fujian Province. H.G. thanks the US National Science Foundation (Grant Nos. CHE-1951328 and CHE-2306975) for support. The computations were performed at the Hefei Advanced Computing Center and Supercomputing Center of Fujian. H.G. thanks Geert-Jan Kroes for his interest in this system and for many useful discussions.

REFERENCES

(1) Schwach, P.; Pan, X.; Bao, X. Direct conversion of methane to value-added chemicals over heterogeneous catalysts: Challenges and prospects. *Chem. Rev.* **2017**, *117*, 8497−8520.

(2) Wang, Y.; Hu, P.; Yang, J.; Zhu, Y.-A.; Chen, D. C−H bond activation in light alkanes: a theoretical perspective. *Chem. Soc. Rev.* **2021**, *50*, 4299−4358.

(3) Chorkendorff, I.; Niemantsverdriet, J. W. *Concepts of Modern Catalysis and Kinetics*; Wiley-VCH: Weinheim, 2003.

(4) Luntz, A. C. Dynamics of Gas-Surface Interactions. In *Surface and Interface Sciences: Solid-Gas Interface II*, Wandelt, K., Ed.; Wiley-VCH Verlag: 2016.

(5) Juurlink, L. B. F.; Killelea, D. R.; Utz, A. L. State-resolve probes of methane dissociation dynamics. *Prog. Surf. Sci.* **2009**, *84*, 69−134.

(6) Chadwick, H.; Beck, R. D. Quantum state−resolved studies of chemisorption reactions. *Annu. Rev. Phys. Chem.* **2017**, *68*, 39−61.

(7) Guo, H.; Farjamnia, A.; Jackson, B. Effects of lattice motion on dissociative chemisorption: Toward a rigorous comparison of theory with molecular beam experiments. *J. Phys. Chem. Lett.* **2016**, *7*, 4576−4584.

(8) Jiang, B.; Yang, M.; Xie, D.; Guo, H. Quantum dynamics of polyatomic dissociative chemisorption on transition metal surfaces: Mode specificity and bond selectivity. *Chem. Soc. Rev.* **2016**, *45*, 3621−3640.

(9) Seets, D. C.; Wheeler, M. C.; Mullins, C. B. Trapping-mediated and direct dissociative chemisorption of methane on Ir(110): A comparison of molecular beam and bulb experiments. *J. Chem. Phys.* **1997**, *107*, 3986−3998.

(10) Seets, D. C.; Reeves, C. T.; Ferguson, B. A.; Wheeler, M. C.; Mullins, C. B. Dissociative chemisorption of methane on Ir(111): Evidence for direct and trapping-mediated mechanisms. *J. Chem. Phys.* **1997**, *107*, 10229−10241.

(11) Jachimowski, T. A.; Hagedorn, C. J.; Weinberg, W. H. Direct and trapping-mediated dissociative chemisorption of methane on Ir(111). *Surf. Sci.* **1997**, *393*, 126−134.

(12) Dombrowski, E.; Peterson, E.; Del Sesto, D.; Utz, A. L. Precursor-mediated reactivity of vibrationally hot molecules: Methane activation on Ir(111). *Catal. Today* **2015**, *244*, 10−18.

(13) Sitz, G. O.; Mullins, C. B. Molecular dynamics simulations of the influence of surface temperature on the trapping of methane on iridium single-crystalline surfaces. *J. Phys. Chem. B* **2002**, *106*, 8349−8353.

(14) Moiraghi, R.; Lozano, A.; Busnengo, H. F. Theoretical study of the dissociative adsorption of methane on Ir(111): The role of steps and surface distortions at high temperatures. *J. Phys. Chem. C* **2016**, *120*, 3946−3954.

(15) Zhou, X.; Jiang, B.; Guo, H. Dissociative chemisorption of methane on stepped Ir(332) surface: Density functional theory and ab initio molecular dynamics studies. *J. Phys. Chem. C* **2019**, *123*, 20893−20902.

(16) Moiraghi, R.; Lozano, A.; Peterson, E.; Utz, A.; Dong, W.; Busnengo, H. F. Nonthermalized precursor-mediated dissociative chemisorption at high catalysis temperatures. *J. Phys. Chem. Lett.* **2020**, *11*, 2211−2218.

(17) Zhou, X.; Zhang, Y.; Guo, H.; Jiang, B. Towards bridging the structure gap in heterogeneous catalysis: the impact of defects in dissociative chemisorption of methane on Ir surfaces. *Phys. Chem. Chem. Phys.* **2021**, *23*, 4376−4385.

(18) Henkelman, G.; Jónsson, H. Theoretical calculations of dissociative adsorption of CH_4 on an Ir(111) surface. *Phys. Rev. Lett.* **2001**, *86*, 664−667.

(19) Jackson, B. Direct and trapping-mediated pathways to dissociative chemisorption: CH_4 dissociation on Ir(111) with step defects. *J. Chem. Phys.* **2020**, *153*, No. 034704.
(20) Walker, A. V.; King, D. A. Dynamics of dissociative methane adsorption on metals: CH_4 on Pt{110}(1x2). *Phys. Rev. Lett.* **1999**, *82*, 5156−5159.
(21) Walker, A. V.; King, D. A. Dynamics of dissociative methane adsorption on metals: CH_4 on Pt{110}(1x2). *J. Chem. Phys.* **2000**, *112*, 4739.
(22) Bisson, R.; Sacchi, M.; Beck, R. D. State-resolved reactivity of CH_4 on Pt(110)-(1x2): The role of surface orientation and impact site. *J. Chem. Phys.* **2010**, *132*, No. 094702.
(23) Bisson, R.; Sacchi, M.; Beck, R. D. Mode-specific reactivity of CH_4 on Pt(110)-(1x2): The concerted role of stretch and bend excitation. *Phys. Rev. B* **2010**, *82*, No. 121404.
(24) Chadwick, H.; Gutiérrez-González, A.; Beck, R. D.; Kroes, G.-J. Transferability of the SRP32-vdW specific reaction parameter functional to CHD_3 dissociation on Pt(110)-(2 × 1). *J. Chem. Phys.* **2019**, *150*, No. 124702.
(25) Anghel, A. T.; Wales, D. J.; Jenkins, S. J.; King, D. A. Pathways for dissociative methane chemisorption on Pt{110}-(1x2). *Phys. Rev. B* **2005**, *71*, No. 113410.
(26) Nave, S.; Tiwari, A. K.; Jackson, B. Methane dissociation and adsorption on Ni(111). Pt(111), Ni(100), Pt(100) and Pt(110)-(1x2): Energetic study. *J. Chem. Phys.* **2010**, *132*, No. 054705.
(27) Han, D.; Nave, S.; Jackson, B. Dissociative chemisorption of methane on Pt(110)-(1×2): Effects of lattice motion on reactions at step edges. *J. Phys. Chem. A* **2013**, *117*, 8651−8659.
(28) Peludhero, I. F.; Gutiérrez-González, A.; Dong, W.; Beck, R. D.; Busnengo, H. F. Dissociative sticking probability of methane on Pt(110)-(2×1). *J. Phys. Chem. C* **2021**, *125*, 11904−11915.
(29) Wei, F.; Smeets, E. W. F.; Voss, J.; Kroes, G.-J.; Lin, S.; Guo, H. Assessing density functionals for describing methane dissociative chemisorption on Pt(110)-(2×1) surface. *Chin. J. Chem. Phys.* **2021**, *34*, 883−895.
(30) Klimeš, J.; Bowler, D. R.; Michaelides, A. Chemical accuracy for the van der Waals density functional. *J. Phys.: Condens. Matter* **2010**, *22*, No. 022201.
(31) Sun, J.; Haunschild, R.; Xiao, B.; Bulik, I. W.; Scuseria, G. E.; Perdew, J. P. Semilocal and hybrid meta-generalized gradient approximations based on the understanding of the kinetic-energy-density dependence. *J. Chem. Phys.* **2013**, *138*, No. 044113.
(32) Smeets, E. W. F.; Kroes, G.-J. Performance of made simple meta-GGA functionals with rVV10 nonlocal correlation for H_2 + Cu(111), D_2 + Ag(111), H_2 + Au(111), and D_2 + Pt(111). *J. Phys. Chem. C* **2021**, *125*, 8993−9010.
(33) Blöchl, P. E. Projector augmented-wave method. *Phys. Rev. B* **1994**, *50*, 17953−17979.
(34) Monkhorst, H. J.; Pack, J. D. Special points for Brillouin-zone integrations. *Phys. Rev. B* **1976**, *13*, 5188−5192.
(35) Henkelman, G.; Uberuaga, B. P.; Jónsson, H. A climbing image nudged elastic band method for finding saddle points and minimum energy paths. *J. Chem. Phys.* **2000**, *113*, 9901−9904.
(36) Kresse, G.; Furthmuller, J. Efficient iterative schemes for ab initio total-energy calculations using plane wave basis set. *Phys. Rev. B* **1996**, *54*, 11169−11186.
(37) Kresse, G.; Furthmuller, J. Efficiency of ab initio total energy calculations for metals and semiconductors using plane wave basis set. *Comput. Mater. Sci.* **1996**, *6*, 15−50.
(38) Zhang, Y.; Hu, C.; Jiang, B. Embedded atom neural network potentials: Efficient and accurate machine learning with a physically inspired representation. *J. Phys. Chem. Lett.* **2019**, *10*, 4962−4967.
(39) Jiang, B.; Li, J.; Guo, H. High-fidelity potential energy surfaces for gas phase and gas-surface scattering processes from machine learning. *J. Phys. Chem. Lett.* **2020**, *11*, 5120−5131.
(40) Zhang, Y.; Lin, Q.; Jiang, B. Atomistic neural network representations for chemical dynamics simulations of molecular, condensed phase, and interfacial systems: Efficiency, representability, and generalization. *WIREs Comput. Mol. Sci.* **2023**, *13*, No. e1645.
(41) Raff, L. M.; Komanduri, R.; Hagan, M.; Bukkapatnam, S. T. S. *Neural Networks in Chemical Reaction Dynamics*; Oxford University Press: Oxford, 2012.
(42) Jiang, B.; Guo, H. Dynamics of water dissociative chemisorption on Ni(111): Effects of impact sites and incident angles. *Phys. Rev. Lett.* **2015**, *114*, No. 166101.
(43) Hase, W. L.; Duchovic, R. J.; Hu, X.; Komornicki, A.; Lim, K. F.; Lu, D.-H.; Peslherbe, G. H.; Swamy, K. N.; Linde, S. R. V.; Varandas, A.; Wang, H.; Wolf, R. J. VENUS96: A General Chemical Dynamics Computer Program. *Quant. Chem. Prog. Exch. Bull.* **1996**, *16*, 671.
(44) Pedregosa, F.; Varoquaux, G.; Gramfort, A.; Michel, V.; Thirion, B.; Grisel, O.; Blondel, M.; Prettenhofer, P.; Weiss, R.; Dubourg, V. Scikit-learn: Machine learning in Python. *J. Mach. Learn. Res* **2011**, *12*, 2825−2830.
(45) Nattino, F.; Ueta, H.; Chadwick, H.; van Reijzen, M. E.; Beck, R. D.; Jackson, B.; van Hemert, M. C.; Kroes, G.-J. Ab initio molecular dynamics calculations versus quantum-state-resolved experiments on CHD_3 + Pt(111): New insights into a prototypical gas−surface reaction. *J. Phys. Chem. Lett.* **2014**, *5*, 1294−1299.
(46) Gutiérrez-González, A.; Torio, M. E.; Busnengo, H. F.; Beck, R. D. Site selective detection of methane dissociation on stepped Pt surfaces. *Top. Catal.* **2019**, *62*, 859−873.
(47) Zambelli, T.; Wintterlin, J.; Trost, J.; Ertl, G. Identification of the "active sites" of a surface-catalyzed reaction. *Science* **1996**, *273*, 1688−1690.
(48) Behrens, M.; Studt, F.; Kasatkin, I.; Kühl, S.; Hävecker, M.; Abild-Pedersen, F.; Zander, S.; Girgskies, F.; Kurr, P.; Kniep, B.-L.; Tovar, M.; Fisher, R. W.; Nørskov, J. K.; Schlögl, R. The active site of methanol synthesis over $Cu/ZnO/Al_2O_3$ industrial catalysts. *Science* **2012**, *336*, 893−897.

https://doi.org/10.1021/jacsau.3c00387
JACS Au 2023, 3, 2835−2843